



Study of $\Lambda_c(2595)$, $\Lambda_c(2625)$, $\Sigma_c(2455)$ and $\Sigma_c(2520)$ Baryons at CDF

The CDF Collaboration
URL <http://www-cdf.fnal.gov>
(Dated: August 12, 2010)

We report a measurement of the resonance properties of $\Lambda_c(2595)^+$ and $\Lambda_c(2625)^+$ in its decays to $\Lambda_c^+ \pi^+ \pi^-$ as well as $\Sigma_c(2455)^{+,0}$ and $\Sigma_c(2520)^{+,0}$ in its decays to $\Lambda_c^+ \pi^\pm$. The measurement is performed using 5.2 fb^{-1} of integrated luminosity from $p\bar{p}$ collisions at $\sqrt{s} = 1.96 \text{ TeV}$, collected with the CDF II detector at the Fermilab Tevatron. Exploiting the largest available sample in the world, we measure masses and widths which are competitive to the world averages for Σ_c states and significantly more precise than the world averages for excited Λ_c states.

Preliminary Results for Summer 2010 Conferences

I. INTRODUCTION

Heavy quark baryons provide, in the same way as heavy quark mesons, an interesting laboratory for studying and testing Quantum Chromodynamics (QCD), the theory of strong interactions. Heavy quark mesons are the closest analogy to the hydrogen atom, which provided important tests of Quantum Electrodynamics. In this analogy we can consider the heavy quark meson as the "hydrogen atom" of QCD. Heavy quark baryons are the next step, where we have a state with one heavy quark and two light quarks, which are often treated together as diquark and so effectively provide the same laboratory as heavy quark mesons. The heavy quark states test regions of the QCD, where perturbation calculations cannot be used and many different approaches to solve the theory were developed. Just a few examples of them are heavy quark effective theory, non-relativistic and relativistic potential models or lattice QCD. While theory is more precise for hadrons containing a b -quark, thanks to much higher statistics experiments can currently provide more precise information on hadrons containing a c -quark. In this note we concentrate on $\Lambda_c(2595)$, $\Lambda_c(2625)$, $\Sigma_c(2455)$ and $\Sigma_c(2520)$ baryons.

On theory side, many different predictions exist on both charm and bottom baryons. In table I we summarize some examples using different approaches. For completeness, Ref. [1] uses a bag model, Refs. [2] and [3, 4] are based on the quark model, Ref. [5] uses QCD sum rules and finally Ref. [6] uses lattice QCD for their prediction. There are few

Hadron	[1]	[2]	[5]	[3, 4]	[6]
$\Sigma_c(2455)$	2393	2455	2400 ± 310	2439	2452
$\Sigma_c(2520)$	2489	2519	2560 ± 240	2518	2538
$\Lambda_c(2595)$	-	2625	2530 ± 220	2598	-
$\Lambda_c(2625)$	-	2636	2580 ± 240	2628	-

TABLE I. Few examples of theory predictions for masses of the charm baryons under study. All numbers are given in MeV/c^2 .

calculations which predict the $\Sigma_c(2455)$ width in the region of $1\text{-}3 \text{ MeV}/c^2$ [7–12] and the $\Sigma_c(2520)$ width to be about $18 \text{ MeV}/c^2$ [12]. For $\Lambda_c(2595)$ and $\Lambda_c(2625)$ up to our current knowledge there are no predictions for the natural widths.

On the experimental side, all four states were observed before and some of their properties measured. Omitting Σ_c^+ states, which cannot be detected by the CDF detector, we list the world average masses and widths in table II [13]. For $\Sigma_c(2455)$ many different measurements exist with most of the information coming from CLEO [14] and FOCUS [15]. Experimental information on the $\Sigma_c(2520)$ state comes practically exclusively from CLEO [16, 17]. It is worth to note that the two CLEO results on $\Sigma_c(2520)$ give inconsistent masses. For the $\Lambda_c(2595)$ and $\Lambda_c(2625)$ three experiments contributed up to now, namely ARGUS [18], E687 at Fermilab [19] and CLEO [20]. In all three cases, their statistics is rather low. Again, the mass of the $\Lambda_c(2625)$ is not consistent between the different experiments. In addition, Blechman and co-workers showed that a more sophisticated treatment, which would take into account the proximity of the threshold in the $\Lambda_c(2595)$ decay, yields a $\Lambda_c(2595)$ mass which is $2\text{-}3 \text{ MeV}/c^2$ below the one derived by the experiments [21]. Σ_c states were observed and studied in $\Lambda_c\pi$ decays, while excited Λ_c states decay mainly to a $\Lambda_c\pi\pi$ final state and decays through intermediated Σ_c resonances are possible. One peculiarity of the experimental studies of these baryons is in their cross talks, which requires special care in the treatment of the background due to different kinematic regions allowed for different sources.

In this analysis we exploit a large sample of $\Lambda_c^+ \rightarrow pK^-\pi^+$ [22] decays collected by the CDF detector to perform the measurement of the masses and widths of the discussed charmed baryons. We take into account all cross-talks and threshold effects expected in the decays under study. The note is organized as follows. In section II we shortly describe the CDF detector and trigger components important for this analysis. The candidate reconstruction is subject to section III and the selection to section IV. After that, in section V we provide details of the fit which is followed by

Hadron	ΔM [MeV/c^2]	Γ [MeV/c^2]
$\Sigma_c(2455)^{++}$	167.56 ± 0.11	2.23 ± 0.3
$\Sigma_c(2455)^0$	167.30 ± 0.11	2.2 ± 0.4
$\Sigma_c(2520)^{++}$	231.9 ± 0.6	14.9 ± 1.9
$\Sigma_c(2520)^0$	231.6 ± 0.5	16.1 ± 2.1
$\Lambda_c(2595)^+$	308.9 ± 0.6	$3.6_{-1.3}^{+2.0}$
$\Lambda_c(2625)^+$	341.7 ± 0.6	< 1.9

TABLE II. World average values for the mass differences ΔM of the studied charm hadrons to Λ_c^+ and their natural widths Γ [13].

the discussion of systematic uncertainties in section VI. Finally, the results are presented in section VII after which we conclude in section VIII.

II. CDF DETECTOR AND TRIGGER

From the components and capabilities of the CDF II detector [23] the tracking system is the one most relevant for this analysis. It lies within a uniform, axial magnetic field of 1.4 T strength. The inner tracking volume up to a radius of 28 cm is filled with 6 – 7 layers of double-sided silicon microstrip detectors [24]. An additional layer of single-sided silicon is mounted directly to the beam-pipe at a radius of 1.5 cm, providing an excellent resolution of the impact parameter d_0 , defined as the distance of closest approach of the track to the interaction point in the transverse plane. The remainder of the tracking volume up to a radius of 137 cm is occupied with an open-cell drift chamber (COT) [25]. Hadron identification is crucial for distinguishing slow kaons and protons from pions. It is provided by a likelihood combination of the ionization energy loss in the COT and a measurement by a time-of-flight system (TOF) [26].

A three-level trigger system is used for the online event selection. The most important part for this analysis at level 1 is the extremely fast tracker (XFT) [27]. Its role is to find tracks of charged particles using information from the COT and measuring their transverse momenta and azimuthal angles around the beam direction. The core of level 2 is the silicon vertex trigger (SVT) which takes XFT tracks as input and add information from SVX, thus allowing the precise measurement of impact parameters of tracks. At level 3, a computing farm running a speed optimized version of the offline software provides the final online selection. The basic requirements at level 1 are two tracks with transverse momentum p_T larger than 2 GeV/c. At level 2, the two tracks are required to have impact parameters in the plane transverse to the beamline in the region of 100 μm to 1 mm and should be consistent with coming from a single vertex displaced by at least 100 μm in the plane transverse to the beamline. Level 3 confirms this selection using a more precise offline type reconstruction. The trigger itself is designed for b -hadrons, but has reasonable efficiency also on c -hadrons. The sample collected for this analysis consists of approximately equal contributions of charm baryons coming from Λ_b decays and direct $c\bar{c}$ production.

III. DATASET AND RECONSTRUCTION

The analysis is performed on the dataset which was collected by the CDF II detector at the Tevatron $p\bar{p}$ collider between February 2002 and June 2009 and corresponds to an integrated luminosity of 5.2 fb⁻¹. The data was cumulated using the displaced track trigger described in the previous section.

The offline reconstruction of candidates starts with track refitting using pion, kaon and proton mass hypotheses to properly take into account differences in the multiple scattering and ionization energy losses. We require that all tracks used in the analysis have a p_T larger than 350 MeV/c. In the second step, three tracks, one with pion, one with kaon and the last one with proton mass hypothesis, are combined to a Λ_c candidate. The three tracks are subject to a kinematical fit which constraints them to originate from a common vertex. We require that the proton and pion candidates have the same charge and that the total charge is ± 1 . The three track invariant mass has to be between 2.2 and 2.38 GeV/ c^2 and the χ^2 of the fit to be less than 20. Finally, we require that two of the tracks used to form the Λ_c candidate are consistent with the trigger requirement. To construct $\Sigma_c(2455)$ and $\Sigma_c(2520)$ candidates we combine each Λ_c candidate with one of the remaining tracks in the event using the pion mass hypothesis. The four tracks are subject to a kinematical fit with appropriate vertex topology constraint. We retain candidates with an invariant mass between 2.3 and 2.65 GeV/ c^2 and a χ^2 of the fit below 100. The $\Lambda_c(2595)$ and $\Lambda_c(2625)$ candidates are obtained by combining each Λ_c candidate with all possible pairs of remaining tracks using the pion mass hypothesis for both of them and subject the candidates to a kinematical fit with appropriate vertex topology constraint. We retain all combinations which have an invariant mass between 2.4 and 2.8 GeV/ c^2 and a χ^2 of the fit below 100.

We use simulated events to estimate the detector resolutions. As the resolution is mainly determined by kinematics and just a tiny fraction of $c\bar{c}$ events passes the trigger requirements, we generate only one sample starting with Λ_b , where the Λ_b kinematics is generated in a way to match the momentum distributions of our total sample. The generated particles are then inclusively decayed by EVTGEN [28] into all possible charm baryons, which are further decayed to the studied channels. In a final step, the Λ_c is forced to decay into $pK^-\pi^+$ with its resonance structure taken into account. Afterwards, the generated events are passed through the detector simulation. As the trigger selection is rather inefficient for Λ_c , we do not run the trigger simulation, but rather imitate the kinematical selection using quantities from offline reconstruction. After detector simulation, the events are reconstructed by the same reconstruction software as used for data.

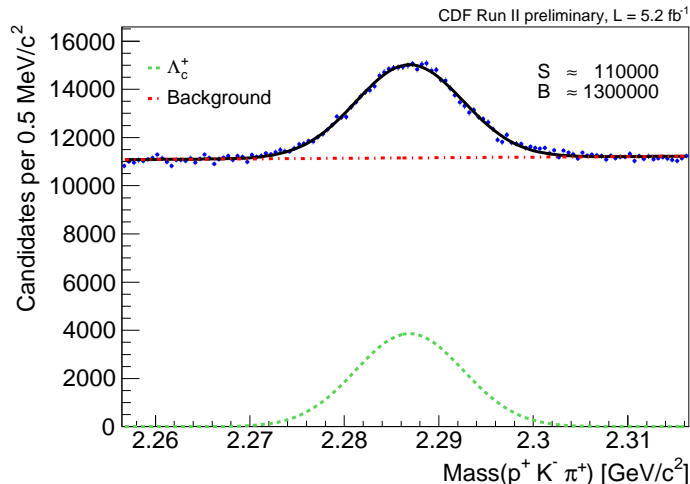


FIG. 1. The invariant mass distribution of Λ_c candidates used to train one of the two neural networks for Λ_c selection.

IV. CANDIDATE SELECTION

The selection of the candidates is done in two steps. In each step we first employ some quality requirements and some requirements to remove the most obvious background. For the remaining candidates we use a neural network to distinguish signal from background. As all final states feature a Λ_c daughter, as first step we perform a Λ_c selection. In the second step we perform a dedicated selection for the four states we study in this work. All neural networks are constructed using the NeuroBayes package [29, 30]. The output of the neural networks from this package is defined to be between -1 and 1 . All neural networks are trained using data only by means of the $sPlot$ technique [31, 32]. This technique assigns a weight to each candidate that the candidate is signal, based on the discriminating variables, which are required to be orthogonal to the ones used in the neural network. In our case, the discriminating variable is the invariant mass of the candidate. In the training each candidate enters with a weight calculated from the signal probability that is derived from its invariant mass. Based on these weights the neural network can learn the features of signal and background events. Additionally, as we use only data for the neural network trainings, for each case we split the sample to two parts (odd and even event numbers) and train two networks. Each of them is applied to the orthogonal subsample in order to maintain a selection which is trained on a sample independent from the one to which we apply it.

A. Λ_c selection

The Λ_c candidates entering into the neural network are required to have at least 10 axial and 10 stereo hits in the COT for each daughter track, p_T of the tracks larger than 400 MeV/c and for protons larger than 1.9 GeV/c, a χ^2 of the kinematical fit smaller than 22 and a displacement of the secondary vertex in the plane transverse to the beam, L_{xy} , larger than 0.25 mm. In addition, we utilize particle identification information from TOF and dE/dx from COT. We combine the two sources of information into a single variable

$$LL_i(p) = \frac{P_{dE/dx}^i(p)P_{TOF}^i(p)}{\sum_{j=\pi,K,p} f_j P_{dE/dx}^j(p)P_{TOF}^j(p)}, \quad (1)$$

where the index i denotes the hypothesis for particle p . The $P_{TOF}^i(p)$ is the probability density to observe the measured TOF given a particle of type i and correspondingly $P_{dE/dx}^i(p)$ the probability density to obtain the measurement of dE/dx . The fractions f_j used in the analysis are $f_\pi = 0.7$, $f_K = 0.2$ and $f_p = 0.1$. We place the requirement $LL_p > 0.6$ on the proton track and $LL_K > 0.2$ on the kaon track. In case neither TOF nor dE/d is available for a given track, we do not place the corresponding requirement and keep the candidate with a special value of the corresponding LL_i quantities. The invariant mass distribution of the candidates with even event numbers is shown in Fig. 1. The fit with a Gaussian function for signal and a linear function for background defines probability density functions (PDFs) used to calculate $sPlot$ weights.

Index	Variable	Index	Variable
1	$LL_p(p)$	8	$p_T(p)$
2	$\sigma_{Lxy}(\Lambda_c)$	9	$\sphericalangle(\Lambda_c, K)$
3	$LL_K(K)$	10	$p_T(\pi)$
4	$\sphericalangle(\Lambda_c, p)$	11	$ d_0/\sigma_{d_0}(K) $
5	$\chi^2(\Lambda_c)$	12	$p_T(K)$
6	$Lxy(\Lambda_c)$	13	$ d_0/\sigma_{d_0}(p) $
7	$ d_0/\sigma_{d_0}(\pi) $		

TABLE III. Inputs to the neural network for the Λ_c^+ selection sorted by their importance.

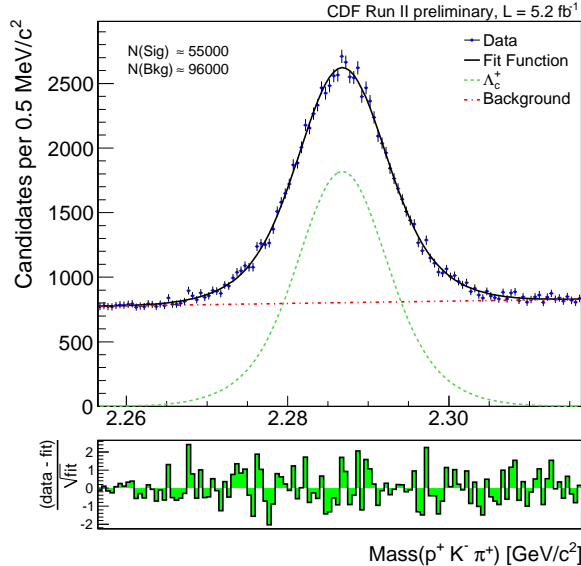


FIG. 2. The invariant mass distribution of Λ_c candidates after requiring their neural network output to be larger than -0.5 .

The final Λ_c selection is performed by means of a neural network. The full list of input quantities sorted by their importance can be found in table III. In the table, $|d_0|$ denotes the impact parameter with respect to the primary vertex of the $p\bar{p}$ interaction for a track in the plane transverse to the beam direction, σ_{d_0} its uncertainty and $\sphericalangle(\Lambda_c, t)$ the cosine of the angle between the directions of the momentum of the Λ_c candidate in the lab frame and the momentum of the proton or kaon track in the center of mass frame of the Λ_c . These angles carry information about the resonant substructure of the decay $\Lambda_c^+ \rightarrow p^+ K^- \pi^+$. In order to show the ability of the neural network to classify signal and background, the invariant mass distribution of Λ_c candidates with the requirement that their neural network output is larger than -0.5 is shown in Fig. 2. In the analysis we apply a less stringent requirement, namely -0.95 and use the output of the Λ_c neural network as input to the following stage.

B. $\Sigma_c(2455)$ and $\Sigma_c(2520)$ selection

The $\Sigma_c(2455)$ and $\Sigma_c(2520)$ selection starts with the application of a few soft requirements followed by the use of a neural network. We require the output of the Λ_c neural network to be larger than -0.95 , $p_T(\pi)$ of the added π to be larger than 400 MeV/c, $|d_0(\pi)| < 1.5$ mm and 2276.46 MeV/c² $< M(\Lambda_c) < 2296.46$ MeV/c². These requirements are common for both neutral and doubly charged states. The mass difference $\Delta M = M(\Sigma_c) - M(\Lambda_c)$ distribution of all the $\Lambda_c^+ \pi^+$ and $\Lambda_c^+ \pi^-$ candidates is shown in Fig. 3. In the ΔM definition, $M(\Sigma_c)$ and $M(\Lambda_c)$ are the invariant masses of the Σ_c and Λ_c candidates.

The neural network for the final selection of the $\Sigma_c(2455)$ and $\Sigma_c(2520)$ candidates uses five input quantities. Ordered by their importance, those are the output of the Λ_c^+ neural network $NN(\Lambda_c^+)$, the proper decay time of the Σ_c candidate $t(\Sigma_c) = L_{xy}(\Sigma_c) \cdot M(\Sigma_c)/p_T(\Sigma_c)$, the quality of the kinematical fit of the Σ_c candidate $\chi^2(\Sigma_c)$, the uncertainty of the Σ_c impact parameter in the transverse plane $\sigma_{d_0}(\Sigma_c)$ and the impact parameter in the transverse plane of the slow pion $|d_0(\pi)|$. Here, slow pion denotes the pion from the Σ_c decay. Separate neural networks are used

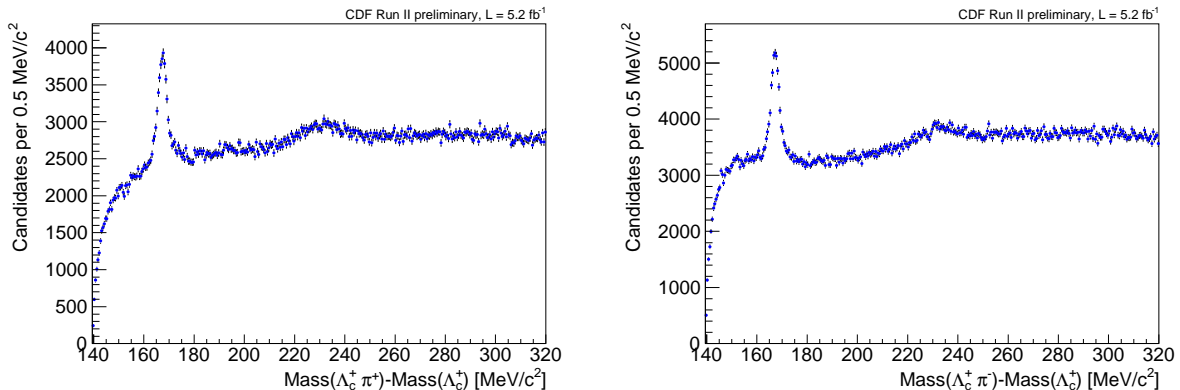


FIG. 3. The mass difference distributions of the $\Lambda_c^+ \pi^+$ (left) and $\Lambda_c^+ \pi^-$ (right) candidates before applying the neural network selection.

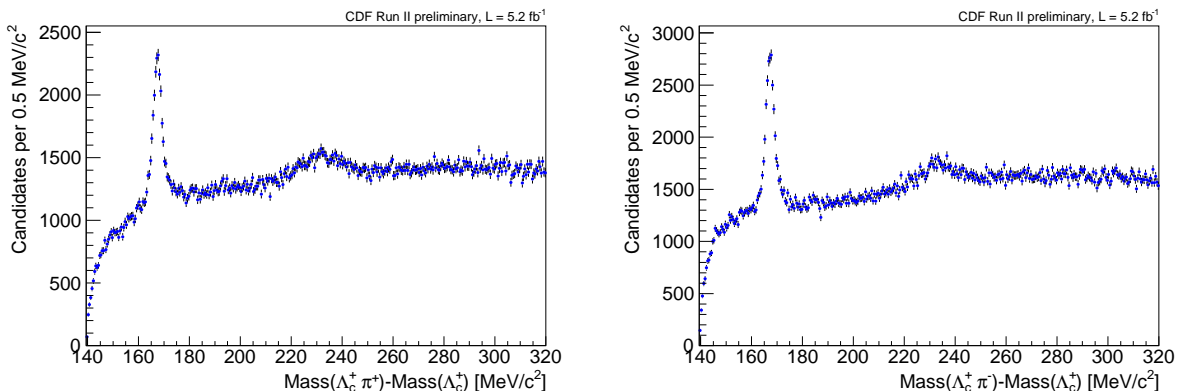


FIG. 4. The mass difference distribution for Σ_c^{++} (left) and Σ_c^0 (right) candidates after the final selection requirements.

for Σ_c^{++} and Σ_c^0 . The training itself is performed using candidates in the mass difference region from $155 \text{ MeV}/c^2$ to $180 \text{ MeV}/c^2$. We choose the requirement on the output of the Σ_c neural network to maximize $S/\sqrt{S+B}$, where S is number of signal Σ_c events and B is number of background events in ΔM between $162.3 \text{ MeV}/c^2$ and $172.3 \text{ MeV}/c^2$. S and B are determined by a fit to the ΔM distribution in the range used for the training employing a Gaussian function for the signal and a linear function for the background. The resulting requirement is the same for both charge combinations. We show the ΔM distributions of the selected candidates in Fig. 4.

C. $\Lambda_c(2595)$ and $\Lambda_c(2625)$ selection

As initial step of the $\Lambda_c(2595)$ and $\Lambda_c(2625)$ selection we require the output of the Λ_c neural network to be larger than -0.95 , $2276.46 \text{ MeV}/c^2 < M(\Lambda_c) < 2296.46 \text{ MeV}/c^2$, $p_T(\pi)$ of both added pions to be larger than $400 \text{ MeV}/c$ and the impact parameter of the object constructed from the two additional pions to be $|d_0(\pi\pi)| < 1.0 \text{ mm}$. The mass difference $\Delta M = M(\Lambda_c^*) - M(\Lambda_c)$ distribution is shown in Fig. 5.

We use the ΔM region between $327 \text{ MeV}/c^2$ and $357 \text{ MeV}/c^2$ for the neural network training. The $sPlot$ weights are based on a Gaussian function for the signal and a linear function for the background PDF. The neural network uses four inputs. Ordered by their importance, those are the quality of the Λ_c^* kinematical fit $\chi^2(\Lambda_c^*)$, the uncertainty of the impact parameter of the combined two pions object $\sigma_{d_0}(\pi\pi)$, the output of the Λ_c neural network $NN(\Lambda_c)$ and the proper decay time of the Λ_c^* . As before, we choose the requirement which maximizes $S/\sqrt{S+B}$. S and B are derived from the fit to the ΔM distribution using a Gaussian function for the signal and a linear function for the background, where we count events in the region $326.7 \text{ MeV}/c^2 < \Delta M < 356.7 \text{ MeV}/c^2$. The resulting mass difference distribution after final requirements can be found in Fig. 6.

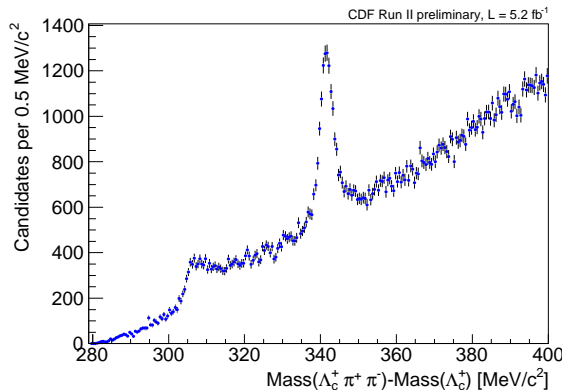


FIG. 5. The mass difference distribution of the $\Lambda_c^+ \pi^+ \pi^-$ candidates before applying the neural network selection.

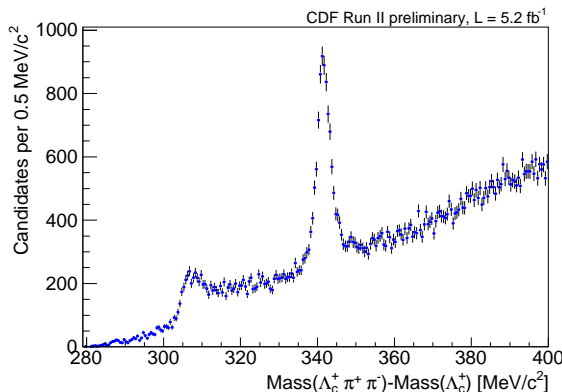


FIG. 6. The mass difference distribution of the $\Lambda_c^+ \pi^+ \pi^-$ candidates with the final selection applied.

V. FIT DESCRIPTION

In order to determine the mass differences relative to the Λ_c and the widths of the six studied states, we perform binned maximum likelihood fits of three separate mass difference distributions. The first two are $\Lambda_c^+ \pi^+$ and $\Lambda_c^+ \pi^-$ which give the states $\Sigma_c(2455)^{+,0}$ and $\Sigma_c(2520)^{+,0}$. The last one is $\Lambda_c^+ \pi^+ \pi^-$ for $\Lambda_c(2595)^+$ and $\Lambda_c(2625)^+$. A complication arises from cross-talks, where in the case of the Σ_c states we need to take into account that a part of the background comes from excited Λ_c decays and thus has different properties as the combinatorial background. On the other hand, when fitting excited Λ_c states, there is a background contribution from random $\Sigma_c^{+,0} \pi^- \pi^+$ combinations which have a threshold close to the $\Lambda_c(2595)^+$ state. In the following, we describe the details of the different fits with their peculiarities.

In all three fits the negative log likelihood function has a general form of

$$\mathcal{L}(\vec{a}) = - \sum_{j=1}^J \ln \left(\frac{\mu_j^{n_j} e^{-\mu_j}}{n_j!} \right) = - \sum_{j=1}^J n_j \ln \mu_j + \sum_{j=1}^J \mu_j + \sum_{j=1}^J \ln(n_j!), \quad (2)$$

where \vec{a} are the free parameters, J is the number of bins in the histogram of the corresponding mass difference distribution, n_j is the number of entries in bin j and μ_j is the expected number of entries in bin j . μ_j is obtained using the function

$$f(\Delta M) = N_1 \cdot s_1(\Delta M) + N_2 \cdot s_2(\Delta M) + b(\Delta M), \quad (3)$$

where N_i is the number of events of the corresponding class, $s_1(\Delta M)$ and $s_2(\Delta M)$ are the PDFs for the two signals and $b(\Delta M)$ is the background function. All three PDFs depend on a subset of the free parameters \vec{a} . The function is evaluated at the bin center when calculating the expectation. While the general structure is the same in all three fits, the PDFs are specific to Σ_c and excited Λ_c states and details are described below.

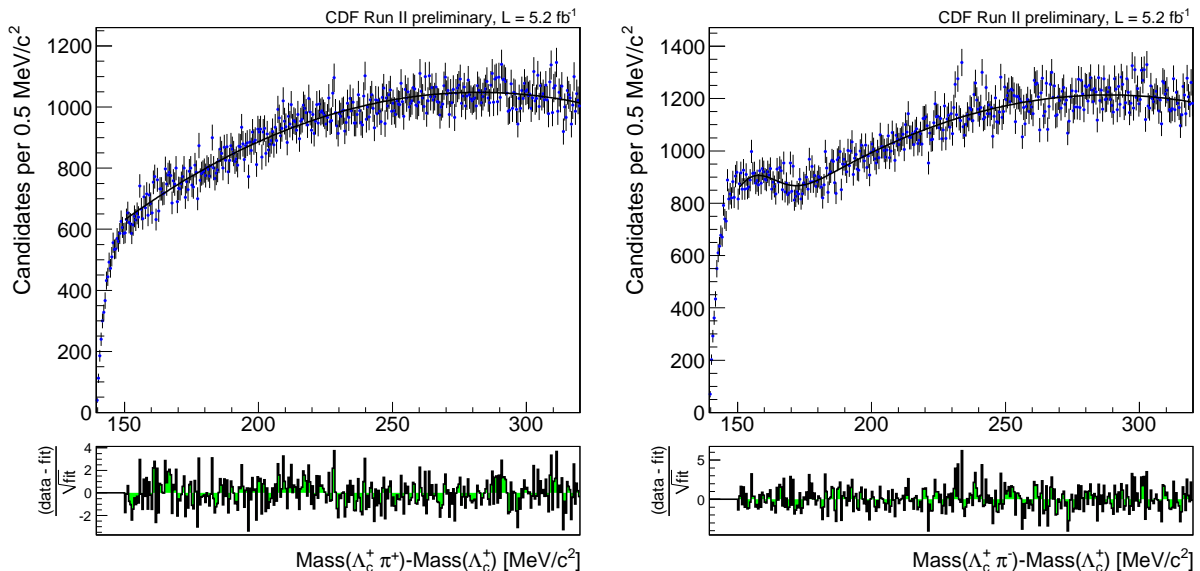


FIG. 7. Fit to the $M(\Lambda_c^+ \pi^+) - M(\Lambda_c^+)$ (left) and $M(\Lambda_c^+ \pi^-) - M(\Lambda_c^+)$ (right) distribution of the candidates from Λ_c mass sidebands.

A. $\Sigma_c(2455)$ and $\Sigma_c(2520)$ fit

In each of the two distributions we need to parametrize two signals and several background components. We use a range from 150 MeV/c^2 to 320 MeV/c^2 . We do not start at threshold to avoid complications arising from the description of the steep rise of background in this region. Both $\Sigma_c(2455)^{++,0}$ and $\Sigma_c(2520)^{++,0}$ are described by a nonrelativistic Breit-Wigner function

$$\frac{dN}{d\Delta M} \propto \frac{1}{2\pi} \cdot \frac{\Gamma}{(\Delta M - \Delta M_0)^2 + \Gamma^2/4} \quad (4)$$

convolved with a resolution function. The resolution function itself is parametrized by a triple Gaussian with mean of all three Gaussians fixed to zero and other parameters derived from simulated events. The mean width of the resolution function is about 1.6 MeV/c^2 for $\Sigma_c(2455)^{++,0}$ and about 2.6 MeV/c^2 for $\Sigma_c(2520)^{++,0}$.

As the width of the resolution function has a significant uncertainty, which will be discussed in the next section, we introduce a single scaling factor s by which the widths of all three Gaussians are multiplied. s is allowed to float within a Gaussian constraint in the fit. Technically this corresponds to adding

$$0.5 \cdot \left(\frac{s - \mu}{\sigma} \right)^2 \quad (5)$$

with $\mu = 1$ and $\sigma = 0.2$ to the negative logarithm of the likelihood.

In the analysis we consider three different types of background, namely random combinations without real Λ_c , combinations of real Λ_c with a random pion and events due to the decay of excited Λ_c to $\Lambda_c^+ \pi^+ \pi^-$. The major part comes from the first source of random combinations without real Λ_c . It is described by a second-order polynomial with shape and amount derived in a fit to the ΔM distribution from Λ_c mass sidebands $2261.46 \text{ MeV}/c^2 < M(\Lambda_c) < 2266.46 \text{ MeV}/c^2$ and $2306.46 \text{ MeV}/c^2 < M(\Lambda_c) < 2311.46 \text{ MeV}/c^2$. In the Σ_c fit, this contribution is allowed to float within a Gaussian constraint implemented by the addition of

$$0.5 \cdot \vec{\Delta}^T \cdot Cov^{-1} \cdot \vec{\Delta}, \quad (6)$$

to the negative logarithm of the likelihood, where Cov is the covariance matrix of the fit to the ΔM distribution from Λ_c mass sidebands and $\vec{\Delta}$ is the vector of parameters of the second-order polynomial. The projections of the fits to the distributions from Λ_c mass sidebands is in Fig. 7. The apparent difference between doubly charged and neutral combinations can be explained by $D^*(2010)^+$ mesons with multibody D^0 decays, where we do not reconstruct all D^0 daughters. In order to describe this reflection, an additional Gaussian function is used. The second background

source consisting of real Λ_c combined with a random pion is modeled by a third-order polynomial. As we do not have an independent proxy for this source, all parameters are left free in the fit. The last source originating from excited Λ_c decays is described using theoretical considerations. With good approximation, there are two states which we need to take into account. Those are $\Lambda_c(2595)$ and $\Lambda_c(2625)$ with both of them decaying into a $\Lambda_c\pi^+\pi^-$ final state. The $\Lambda_c(2595)$ decays dominantly to a $\Sigma_c\pi$ final state [13] and thus contributes mainly to the signal. So we neglect its contribution to nonresonant $\Lambda_c\pi^+\pi^-$. On the other hand, the $\Lambda_c(2625)$ decay is dominantly nonresonant [13]. To model it, we start from the flat $\Lambda_c\pi^+\pi^-$ Dalitz plot and project it on the appropriate axis. Since the shape of the projection depends on the reconstructed $\Lambda_c\pi^+\pi^-$ mass, we use 10 different values of the $\Lambda_c\pi^+\pi^-$ invariant mass and weight their contribution according to the shape we obtain from our $\Lambda_c\pi^+\pi^-$ data.

B. $\Lambda_c(2595)$ and $\Lambda_c(2625)$ fit

As before, also the fit for $\Lambda_c(2595)$ and $\Lambda_c(2625)$ has two signals and several background components. Additional complication compared to the Σ_c case arises from the fact that previous measurements of the $\Lambda_c(2595)$ properties indicate that it decays dominantly to the final state $\Sigma_c\pi$, which has its threshold very close to the $\Lambda_c(2595)$ mass. As we discussed in the introduction, Ref. [21] shows that taking into account the strong variation of the natural width yields masses which are below those measured by the experiments. With the statistics we have available we are much more sensitive to the details of the $\Lambda_c(2595)$ line shape than previous analyses. The fit is performed in a ΔM region from 290 MeV/ c^2 to 400 MeV/ c^2 .

The signal PDF for the $\Lambda_c(2625)$ is the nonrelativistic Breit-Wigner function of equation 4 convolved with a resolution function determined from simulation and consisting of three Gaussians with means fixed to zero. The mean width of the resolution function is about 2.4 MeV/ c^2 . As for the Σ_c case, we introduce a single, Gaussian constraint scaling factor s by which the widths of all three Gaussians are multiplied, in order to account for the uncertainty in the width of the resolution function.

The $\Lambda_c(2595)$ parametrization follows Ref. [21]. The state is described by a nonrelativistic Breit-Wigner function of the form

$$\frac{dN}{d\Delta M} \propto \frac{\Gamma(\Lambda_c^+ \pi^+ \pi^-)}{(\Delta M - \Delta M_{\Lambda_c(2595)})^2 + (\Gamma(\Lambda_c^+ \pi^+ \pi^-) + \Gamma(\Lambda_c^+ \pi^0 \pi^0))^2/4}, \quad (7)$$

where $\Gamma(\Lambda_c^+ \pi^+ \pi^-)$ and $\Gamma(\Lambda_c^+ \pi^0 \pi^0)$ are the partial widths to the $\Lambda_c^+ \pi^+ \pi^-$ and $\Lambda_c^+ \pi^0 \pi^0$ final states. Assuming that those two final states cover most of the total width, the sum in the denominator corresponds to the total width. The two partial widths are defined as

$$\Gamma(\Lambda_c^+ \pi^+ \pi^-) = \frac{g_2^2}{16\pi^3 f_\pi^4} m_{\Lambda_c} \int dE_1 dE_2 (|\vec{p}_2|^2 |A(E_1)|^2 + |\vec{p}_1|^2 |B(E_2)|^2 + 2\vec{p}_1 \cdot \vec{p}_2 \text{Re}[A(E_1)B^*(E_2)]), \quad (8)$$

$$\Gamma(\Lambda_c^+ \pi^0 \pi^0) = \frac{g_2^2}{16\pi^3 f_\pi^4} m_{\Lambda_c} \int dE_1 dE_2 (|\vec{p}_2|^2 |C(E_1)|^2 + |\vec{p}_1|^2 |C(E_2)|^2 + 2\vec{p}_1 \cdot \vec{p}_2 \text{Re}[C(E_1)C^*(E_2)]). \quad (9)$$

Here, $f_\pi = 132 \text{ MeV}/c^2$ is the pion decay constant [33], m_{Λ_c} is the world-average Λ_c mass, E_1, E_2 are the energies of the two pions in the rest frame of the $\Lambda_c(2595)$ and \vec{p}_1, \vec{p}_2 are the corresponding momenta. The coupling constant g_2 is determined by the Σ_c decay width using the relation

$$\Gamma_{\Sigma_c} = \frac{g_2^2}{2\pi f_\pi^2} \frac{m_{\Lambda_c}}{m_{\Sigma_c}} |\vec{p}_\pi|^3 \quad (10)$$

with m_{Σ_c} being the world average mass of the $\Sigma_c(2455)$. From world average $\Gamma_{\Sigma_c} = 2.2 \text{ MeV}/c^2$ we obtain the value $g_2^2 = 0.365$ which is fixed in the fit. A , B and C are amplitudes for the decays $\Lambda_c(2595)^+ \rightarrow \Sigma_c(2455)^0 \pi^+$, $\Lambda_c(2595)^+ \rightarrow \Sigma_c(2455)^{++} \pi^-$ and $\Lambda_c(2595)^+ \rightarrow \Sigma_c(2455)^+ \pi^0$ and are parametrized as

$$A(E) = \frac{h_2 E}{\Delta m - \Delta m_{\Sigma_c^0} - E + i\Gamma_{\Sigma_c^0}/2}, \quad (11)$$

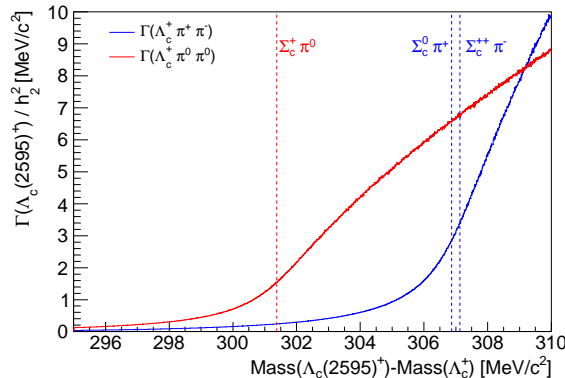


FIG. 8. Calculated dependence of $\Gamma(\Lambda_c^+ \pi^+ \pi^-)$ and $\Gamma(\Lambda_c^+ \pi^0 \pi^0)$ on $M(\Lambda_c(2595)^+) - M(\Lambda_c)$. The constant factor h_2^2 is determined by a fit to the experimental data.

$$B(E) = \frac{h_2 E}{\Delta m - \Delta m_{\Sigma_c^{++}} - E + i\Gamma_{\Sigma_c^{++}}/2}, \quad (12)$$

$$C(E) = \frac{1}{2} \cdot \frac{h_2 E}{\Delta m - \Delta m_{\Sigma_c^+} - E + i\Gamma_{\Sigma_c^+}/2}. \quad (13)$$

In these definitions, $m_{\Sigma_c^{++},+0}$ and $\Gamma_{\Sigma_c^{++},+0}$ are mass and width of the $\Sigma_c^{++},+0(2455)$ taken from Ref. [13]. The coupling constant h_2 is related to the decay width of the $\Lambda_c(2595)$ and represents the quantity we measure instead of the natural width. For illustration we show the dependence of the two partial widths in Fig. 8. The shape defined by equation 7 is then numerically convolved with a three Gaussian resolution function determined from simulation, which has a mean width of about $1.8 \text{ MeV}/c^2$. Again, the means of all three Gaussians are fixed to zero and a single, Gaussian constraint scaling factor s is introduced by which the widths of all three Gaussians are multiplied.

The background consists of three different sources which are combinatorial background without real Λ_c , real Λ_c combined with two random pions and real $\Sigma_c^{++},+0$ combined with a random pion. As in the case of Σ_c , the combinatorial background without real Λ_c is parametrized by a second order polynomial whose parameters are determined in a fit to the ΔM distribution of candidates from the Λ_c mass sidebands $2261.46 \text{ MeV}/c^2 < M(\Lambda_c) < 2266.46 \text{ MeV}/c^2$ and $2306.46 \text{ MeV}/c^2 < M(\Lambda_c) < 2311.46 \text{ MeV}/c^2$. This distribution together with the fit projection can be found in Fig. 9. In the final fit, we keep the parameters for this background floating within a Gaussian constraint of the form of equation 6 to the values found in the fit to the candidates from Λ_c mass sidebands. The second source consisting of real Λ_c combined with two random pions is parametrized by a second order polynomial with all parameters allowed to float in the fit. The final source of background are real Σ_c combined with a random pion. For this source the main issue is to have the proper shape close to the threshold, whereas small imperfections at higher ΔM can be ignored as the second background source has enough flexibility to absorb it. The PDF is based on a uniform function defined from the threshold to the end of the fit range. In order to take into account the natural widths as well as resolution effects, we add together 10 such functions for both $\Sigma_c(2455)^{++}$ and $\Sigma_c(2455)^0$ with thresholds distributed according to the shape derived in the Σ_c fits. The size of this contribution is constrained to the $\Sigma_c(2455)$ yield obtained from the fit to the $M(\Sigma_c) - M(\Lambda_c)$ distribution for candidates with $M(\Lambda_c^*) - M(\Lambda_c) > 355 \text{ MeV}/c^2$. The two distributions together with the fit projections are shown in Fig. 10.

VI. SYSTEMATIC UNCERTAINTIES

We investigate several systematic effects, which can affect our measurements. Generally, they can be categorized as imperfect modeling by the simulation, imperfect knowledge of the momentum scale of the detector, ambiguities in the fit model and uncertainties on the external inputs to the fit. In this section we discuss how they can affect our results and the way we assess the size of the possible effects. A summary of the obtained uncertainties are in tables IV to VI.

In order to properly describe the signal shapes, we need to understand the intrinsic resolution of the detector. We estimate it using simulated events, but several issues can arise in such a process which can be split to several categories. The first one deals with intrinsic difficulties to properly simulate the charge deposition in the detector

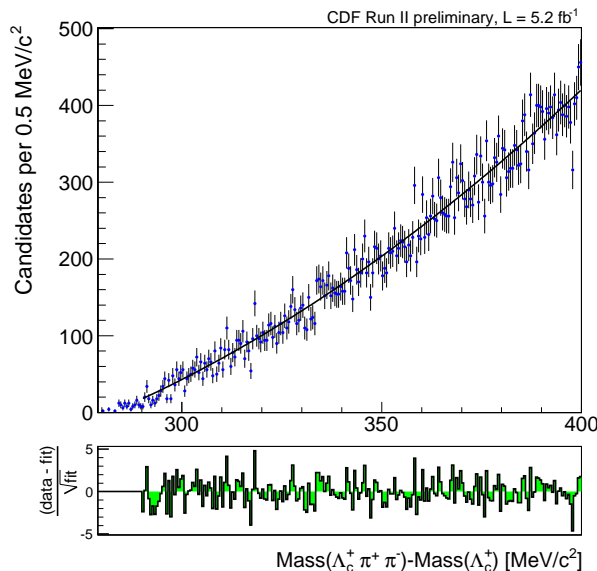


FIG. 9. Fit to the $M(\Lambda_c^+ \pi^+ \pi^-) - M(\Lambda_c^+)$ distribution of the candidates from Λ_c mass sidebands.

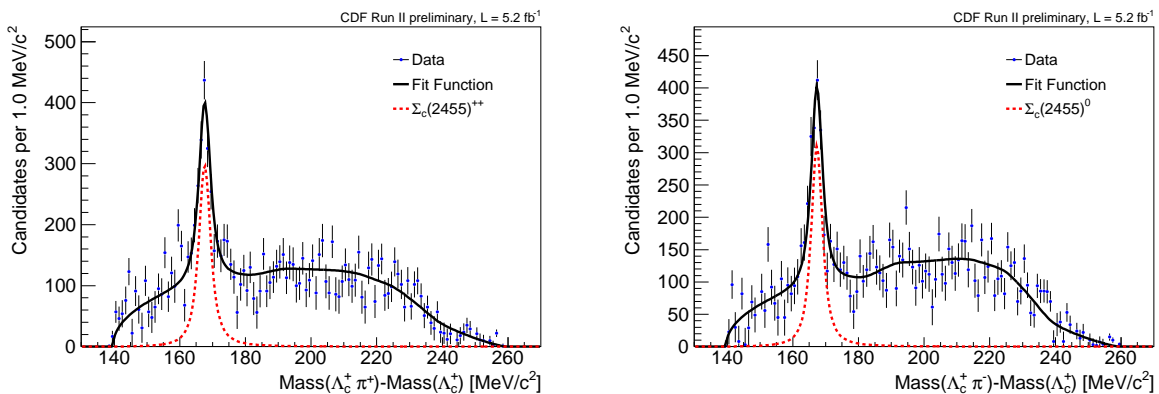


FIG. 10. Distribution of $M(\Sigma_c) - M(\Lambda_c)$ for candidates with $M(\Lambda_c^*) - M(\Lambda_c) > 355 \text{ MeV}/c^2$ together with the fit projection.

and thus providing incorrect uncertainties for the track parameters, which then reflects to a wrong ΔM uncertainty. Second, we make some approximations in order to obtain sufficient statistics using reasonable computing resources. This is motivated by the low efficiency of the triggers, which are not fully simulated. We also simulate just a single source of the studied baryons, namely decays of Λ_b baryons, without the rest of the event. Finally, we do not simulate multiple interactions within a single bunch crossing. We use $D^{*+} \rightarrow D^0 \pi^+$ with $D^0 \rightarrow K \pi$ and $\psi(2S) \rightarrow J/\psi \pi^+ \pi^-$ with $J/\psi \rightarrow \mu^+ \mu^-$ to estimate the effect of those approximations. We compare our data with events simulated with the same approximations as a function of the p_T of the pions added to D^0 or J/ψ and the instantaneous luminosity. We also compare the overall resolution scale between data and simulated events and find that all variations are below 20% which we assign as uncertainty on our knowledge of the resolution function. The contribution from this uncertainty is already included in the uncertainties on the resonance parameters determined by the default fit with Gaussian constraint on the resolution scale factor. To disentangle it from the statistical component, we repeat the fits on data without multiplying the widths of the resolution function by the scale factor s . The systematic uncertainty due to the imperfect modeling of the resolution function is then obtained by the difference in quadrature of the uncertainty of the baseline fit from the uncertainty of the modified fit. As expected, this uncertainty in the resolution has a large impact on the natural widths, but a negligible effect on the mass differences.

The imperfect knowledge of the momentum scale originates from our limited precision with which we measure the magnetic field and the amount of material in the detector. The magnetic field is needed to relate the measured curvature of the tracks to their momentum. Knowledge on the amount of material is important to properly estimate

the energy loss of particles traversing the detector. Both parts are originally calibrated using $J/\psi \rightarrow \mu^+ \mu^-$ decays. The weak point with respect to this analysis is that this calibration uses muons which are required to have $p_T > 1.5$ GeV/ c , while pions from Σ_c or Λ_c^* decays typically have much lower p_T . The estimation of the uncertainty on the mass differences comes from our previous work on $X(3872)$ [34]. There, $\psi(2S) \rightarrow J/\psi \pi^+ \pi^-$ decays are used to study the momentum scale uncertainties by comparing the measured $\psi(2S)$ mass with the world average [13]. In addition, we study $\psi(2S)$ mass dependence on kinematic properties of the pions which put bounds on the size of the possible effects. In addition, in the analysis at hand we verify the momentum scale also using D^{*+} decays with difference to the world average far below the uncertainty derived from $\psi(2S)$. Based on Ref. [34] we assign a 0.12 MeV/ c^2 uncertainty on the mass differences of all states under study due to the imperfect knowledge of the momentum scale. The effect of this source on the natural width was studied in Ref. [35] and we assign the 0.2 MeV/ c^2 found there as uncertainty on the natural width due to the imperfect knowledge of the momentum scale. To translate this uncertainty to the coupling constant h_2 we assign it to $\Gamma(\Lambda_c^+ \pi^+ \pi^-) + \Gamma(\Lambda_c^+ \pi^0 \pi^0)$, which is a function of h_2 , and perform Gaussian error propagation.

In tests of our fit model and procedure we check two effects. The first one is the internal consistency of the fit and the second is the shape of the signal PDFs. We do not perform an explicit check of the background parametrizations as those are described by polynomials and any analytic function can be approximated by a polynomial of sufficient degrees. As the fit quality does not indicate significant discrepancies between data and model we conclude that the degree of the polynomial functions used is sufficient. Some backgrounds are determined from independent sources, but as the appropriate parameters are Gaussian constrained in the fit, the uncertainty originating from limited statistics of the external sources, like Λ_c mass sidebands, is already included in the statistical uncertainties of the results. To check the internal consistency of the fit procedure, we generate a large sample of pseudoexperiments using PDFs of our fit model with parameters obtained from the fit on data. Estimates of all physics parameters but the mass differences and natural widths of the $\Sigma_c(2520)$ resonances are found to be unbiased. The bias on the natural widths can be explained by the flexibility in the background PDF that may absorb low statistics signal tails. To be conservative, we repeat the study with a true value for the $\Sigma_c(2520)$ natural width of below ($\Gamma = 7.5$ MeV/ c^2) and above ($\Gamma = 20$ MeV/ c^2) the measured value and find that the bias has a variation with the true value. The biases are largest for a true value of the natural width of 20 MeV/ c^2 and we assign these biases as systematic uncertainties on the mass differences and natural widths of the $\Sigma_c(2520)$ states. In the case of excited Λ_c states we do not find any bias and conclude that the uncertainty is negligible. For the second effect, the uncertainty on the signal shape, we check whether our signal parametrization using nonrelativistic Breit-Wigner functions provides a proper description. We refit the Σ_c and $\Lambda_c(2625)$ data using P -wave relativistic Breit-Wigner functions of the form

$$\frac{dN}{dm} \propto \frac{m \cdot \Gamma(m)}{(m_0^2 - m^2)^2 + m_0^2 \cdot \Gamma^2(m)} \quad (14)$$

with

$$\Gamma(m) = \Gamma_0 \left(\frac{q}{q_0} \right)^3 \left(\frac{m_0}{m} \right) \left(\frac{1 + q_0^2 R^2}{1 + q^2 R^2} \right), \quad (15)$$

where $m = \Delta M + m_{\Lambda_c}$, R is the Blatt-Weisskopf radius set to 3 (GeV/ c) $^{-1}$ [36, 37], m_0 and Γ_0 are the nominal mass and width and $q(q_0)$ is the momentum of the daughters in the Σ_c or $\Lambda_c(2625)$ rest frame calculated from the actual (nominal) mass. As for the $\Lambda_c(2595)$ a variable width is already taken into account, we only replace the nonrelativistic Breit-Wigner function of equation 7 by a relativistic one. For the $\Sigma_c(2455)$ we observe a difference of 0.02 MeV/ c^2 in the mass difference which we assign as systematic uncertainty. In the cases of $\Sigma_c(2520)$ and excited Λ_c resonances we do not observe any shift and conclude that the effect is negligible.

Finally, the lineshape of the $\Lambda_c(2595)$ depends on the input values of the $\Sigma_c(2455)$ masses and widths and the pion decay constant f_π . We repeat the fit using values of those parameters smaller or larger by one standard deviation and take the largest variation as systematic uncertainty. The effect of the uncertainty on the world average $\Sigma_c(2455)$ masses and widths used as input is dominant compared to the effect of the uncertainty on f_π .

The values of the assigned uncertainties are summarized in tables IV to VI. To obtain the total systematic uncertainties, we add all sources in quadrature.

VII. RESULTS

Putting all ingredients together we perform fits of the $M(\Lambda_c^+ \pi^+) - M(\Lambda_c^+)$, $M(\Lambda_c^+ \pi^-) - M(\Lambda_c^+)$ and $M(\Lambda_c^+ \pi^+ \pi^-) - M(\Lambda_c^+)$ mass difference distributions to obtain the desired resonance properties. In Figs. 11 to 13 we show the measured data distributions together with the fit projections. We see about 13800 $\Sigma_c(2455)^{++}$, 15900 $\Sigma_c(2455)^0$,

Source	$\Delta M(\Sigma_c(2455)^{++})$	$\Gamma(\Sigma_c(2455)^{++})$	$\Delta M(\Sigma_c(2520)^{++})$	$\Gamma(\Sigma_c(2520)^{++})$
Resolution	-	0.40 MeV/c ²	-	0.69 MeV/c ²
Momentum Scale	0.12 MeV/c ²	0.20 MeV/c ²	0.12 MeV/c ²	0.20 MeV/c ²
Fit Model	0.02 MeV/c ²	-	0.11 MeV/c ²	1.16 MeV/c ²
Sum	0.12 MeV/c ²	0.45 MeV/c ²	0.16 MeV/c ²	1.36 MeV/c ²
Statistical	0.04 MeV/c ²	0.13 MeV/c ²	0.56 MeV/c ²	2.12 MeV/c ²

TABLE IV. Systematic uncertainties on the measurements of the mass differences and decay widths of the Σ_c^{++} resonances. The corresponding statistical uncertainties are listed for comparison.

Source	$\Delta M(\Sigma_c(2455)^0)$	$\Gamma(\Sigma_c(2455)^0)$	$\Delta M(\Sigma_c(2520)^0)$	$\Gamma(\Sigma_c(2520)^0)$
Resolution	-	0.45 MeV/c ²	-	0.70 MeV/c ²
Momentum Scale	0.12 MeV/c ²	0.20 MeV/c ²	0.12 MeV/c ²	0.20 MeV/c ²
Fit Model	0.02 MeV/c ²	-	0.11 MeV/c ²	1.16 MeV/c ²
Sum	0.12 MeV/c ²	0.49 MeV/c ²	0.16 MeV/c ²	1.37 MeV/c ²
Statistical	0.03 MeV/c ²	0.11 MeV/c ²	0.43 MeV/c ²	1.82 MeV/c ²

TABLE V. Systematic uncertainties on the measurements of the mass differences and decay widths of the Σ_c^0 resonances. The corresponding statistical uncertainties are listed for comparison.

Source	$\Delta M(\Lambda_c(2595)^+)$	h_2^2	$\Gamma(\Lambda_c(2595)^+)$	$\Delta M(\Lambda_c(2625)^+)$
Resolution	0.06 MeV/c ²	0.03	0.22 MeV/c ²	-
Momentum Scale	0.12 MeV/c ²	0.03	0.20 MeV/c ²	0.12 MeV/c ²
Fit Model	-	-	-	-
$\Delta M, \Gamma$ of $\Sigma_c(2455)$	0.15 MeV/c ²	0.06	0.36 MeV/c ²	-
Sum	0.20 MeV/c ²	0.07	0.47 MeV/c ²	0.12 MeV/c ²
Statistical	0.14 MeV/c ²	0.04	0.30 MeV/c ²	0.04 MeV/c ²

TABLE VI. Systematic uncertainties on the measurements of the mass differences of the excited Λ_c resonances and the pion coupling constant h_2^2 ($\Gamma(\Lambda_c(2595)^+)$). The corresponding statistical uncertainties are listed for comparison.

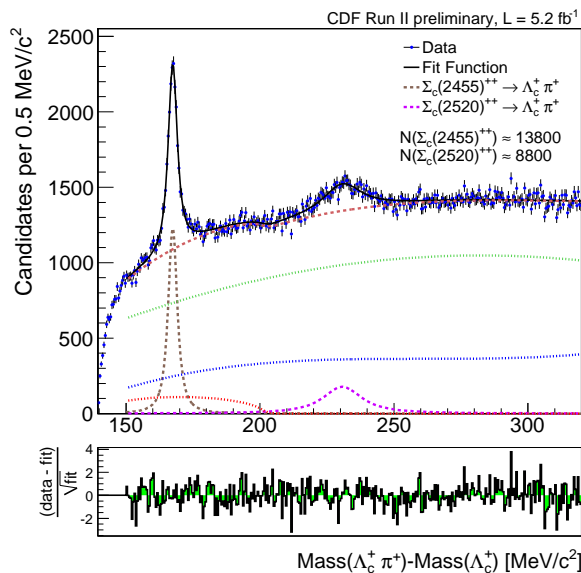


FIG. 11. The $M(\Lambda_c^+ \pi^+) - M(\Lambda_c^+)$ distribution obtained from data (points with error bars) together with the fit projection (black line). The brown and violet lines correspond to the two signal contributions, the green line represents the combinatorial background without real Λ_c , the blue line shows real Λ_c combined with a random pion and the red dotted line represents a reflection from excited Λ_c decays. The red dashed line corresponds to the sum of all three background contributions.

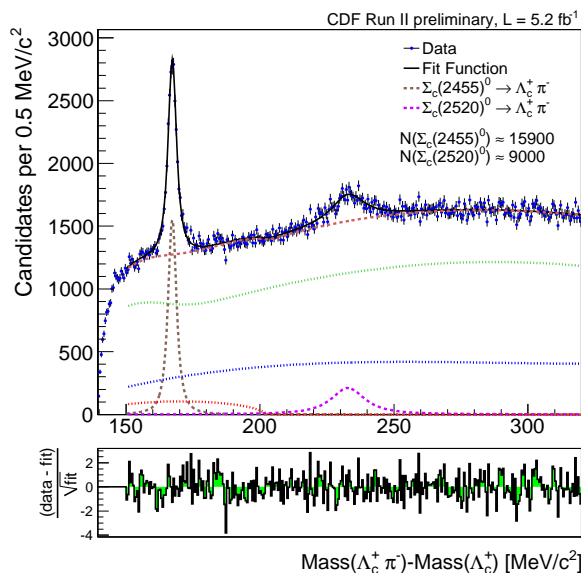


FIG. 12. The $M(\Lambda_c^+ \pi^-) - M(\Lambda_c^+)$ distribution obtained from data (points with error bars) together with the fit projection (black line). The brown and violet lines correspond to the two signal contributions, the green line represents the combinatorial background without real Λ_c , the blue line shows real Λ_c combined with a random pion and the red dotted line represents a reflection from excited Λ_c decays. The red dashed line corresponds to the sum of all three background contributions.

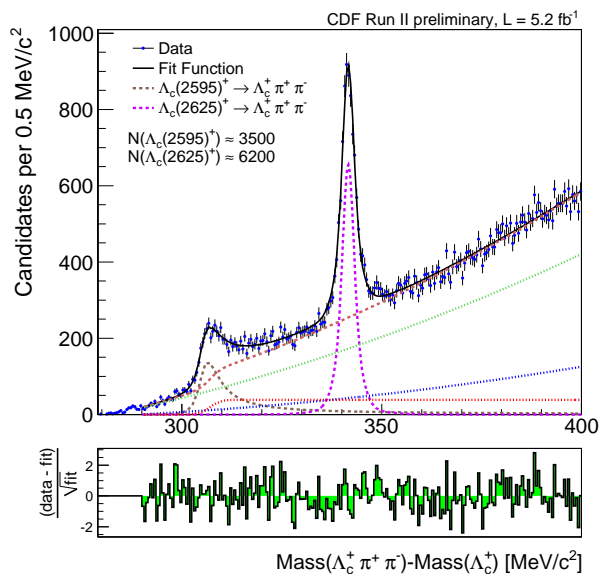


FIG. 13. The $M(\Lambda_c^+ \pi^+ \pi^-) - M(\Lambda_c^+)$ distribution obtained from data (points with error bars) together with the fit projection (black line). The brown and violet lines correspond to the two signal contributions, the green line represents the combinatorial background without real Λ_c , the blue line shows real Λ_c combined with two random pions and the red dotted line represents real Σ_c combined with a random pion. The red dashed line corresponds to the sum of all three background contributions.

8800 $\Sigma_c(2520)^{++}$, 9000 $\Sigma_c(2520)^0$, 3500 $\Lambda_c(2595)^+$ and 6200 $\Lambda_c(2625)^+$ signal events. For the resonance parameters

we obtain

$$\begin{aligned}
\Delta M(\Sigma_c(2455)^{++}) &= 167.44 \pm 0.04 \text{ (stat.)} \pm 0.12 \text{ (syst.) MeV}/c^2, \\
\Gamma(\Sigma_c(2455)^{++}) &= 2.34 \pm 0.13 \text{ (stat.)} \pm 0.45 \text{ (syst.) MeV}/c^2, \\
\Delta M(\Sigma_c(2455)^0) &= 167.28 \pm 0.03 \text{ (stat.)} \pm 0.12 \text{ (syst.) MeV}/c^2, \\
\Gamma(\Sigma_c(2455)^0) &= 1.65 \pm 0.11 \text{ (stat.)} \pm 0.49 \text{ (syst.) MeV}/c^2, \\
\Delta M(\Sigma_c(2520)^{++}) &= 230.73 \pm 0.56 \text{ (stat.)} \pm 0.16 \text{ (syst.) MeV}/c^2, \\
\Gamma(\Sigma_c(2520)^{++}) &= 15.03 \pm 2.12 \text{ (stat.)} \pm 1.36 \text{ (syst.) MeV}/c^2, \\
\Delta M(\Sigma_c(2520)^0) &= 232.88 \pm 0.43 \text{ (stat.)} \pm 0.16 \text{ (syst.) MeV}/c^2, \\
\Gamma(\Sigma_c(2520)^0) &= 12.51 \pm 1.82 \text{ (stat.)} \pm 1.37 \text{ (syst.) MeV}/c^2, \\
\Delta M(\Lambda_c(2595)^+) &= 305.79 \pm 0.14 \text{ (stat.)} \pm 0.20 \text{ (syst.) MeV}/c^2, \\
h_2^2(\Lambda_c(2595)^+) &= 0.36 \pm 0.04 \text{ (stat.)} \pm 0.07 \text{ (syst.)}, \\
\Delta M(\Lambda_c(2625)^+) &= 341.65 \pm 0.04 \text{ (stat.)} \pm 0.12 \text{ (syst.) MeV}/c^2.
\end{aligned}$$

For the width of the $\Lambda_c(2625)$ we obtain a value consistent with zero and therefore calculate an upper limit using a Bayesian approach with a uniform prior restricted to positive values. At the 90% C.L. we obtain $\Gamma(\Lambda_c(2625)^+) < 0.97 \text{ MeV}/c^2$. For easier comparison to previous results, h_2^2 corresponds to $\Gamma(\Lambda_c(2595)^+) = 2.59 \pm 0.30 \pm 0.47 \text{ MeV}/c^2$. Except of $\Delta M(\Lambda_c(2595)^+)$, all measured quantities are in reasonable agreement with previous measurements. For $\Delta M(\Lambda_c(2595)^+)$ we observe a value which is by $3.1 \text{ MeV}/c^2$ smaller than the existing world average. This difference is of the same size as found in Ref. [21]. The precision for the Σ_c states is comparable to the precision of the world averages. In the case of excited Λ_c states our measurements provide a significant improvement on precision against previous measurements. This is mainly driven by about 30-fold larger statistics than observed before.

VIII. CONCLUSIONS

While the CDF detector is optimized for the detection of b -hadrons, it still provides a large amount of c -hadrons. In this paper we exploit the world largest samples of excited charm baryons to measure the resonance parameters of six states, namely $\Sigma_c(2455)^{++}$, $\Sigma_c(2455)^0$, $\Sigma_c(2520)^{++}$, $\Sigma_c(2520)^0$, $\Lambda_c(2595)^+$ and $\Lambda_c(2625)^+$. We obtain the following masses and widths:

$$\begin{aligned}
M(\Sigma_c(2455)^{++}) &= 2453.90 \pm 0.13 \pm 0.14 \text{ MeV}/c^2, \\
\Gamma(\Sigma_c(2455)^{++}) &= 2.34 \pm 0.47 \text{ MeV}/c^2, \\
M(\Sigma_c(2455)^0) &= 2453.74 \pm 0.12 \pm 0.14 \text{ MeV}/c^2, \\
\Gamma(\Sigma_c(2455)^0) &= 1.65 \pm 0.50 \text{ MeV}/c^2, \\
M(\Sigma_c(2520)^{++}) &= 2517.19 \pm 0.46 \pm 0.14 \text{ MeV}/c^2, \\
\Gamma(\Sigma_c(2520)^{++}) &= 15.03 \pm 2.52 \text{ MeV}/c^2, \\
M(\Sigma_c(2520)^0) &= 2519.34 \pm 0.58 \pm 0.14 \text{ MeV}/c^2, \\
\Gamma(\Sigma_c(2520)^0) &= 12.51 \pm 2.28 \text{ MeV}/c^2, \\
M(\Lambda_c(2595)^+) &= 2592.25 \pm 0.24 \pm 0.14 \text{ MeV}/c^2, \\
h_2^2(\Lambda_c(2595)^+) &= 0.36 \pm 0.08, \\
M(\Lambda_c(2625)^+) &= 2628.11 \pm 0.13 \pm 0.14 \text{ MeV}/c^2, \\
\Gamma(\Lambda_c(2625)^+) &< 0.97 \text{ MeV}/c^2 \text{ at 90\% C.L.},
\end{aligned}$$

where the first uncertainty is the experimental one and for the masses the second uncertainty is the one on the world average Λ_c mass. These measurements provide a significant improvement on the knowledge of the resonance parameters for the studied baryons.

ACKNOWLEDGMENTS

We thank the Fermilab staff and the technical staffs of the participating institutions for their vital contributions. This work was supported by the U.S. Department of Energy and National Science Foundation; the Italian Istituto

Nazionale di Fisica Nucleare; the Ministry of Education, Culture, Sports, Science and Technology of Japan; the Natural Sciences and Engineering Research Council of Canada; the National Science Council of the Republic of China; the Swiss National Science Foundation; the A.P. Sloan Foundation; the Bundesministerium für Bildung und Forschung, Germany; the World Class University Program, the National Research Foundation of Korea; the Science and Technology Facilities Council and the Royal Society, UK; the Institut National de Physique Nucleaire et Physique des Particules/CNRS; the Russian Foundation for Basic Research; the Ministerio de Ciencia e Innovación, and Programa Consolider-Ingenio 2010, Spain; the Slovak R&D Agency; and the Academy of Finland.

-
- [1] A. Bernotas and V. Simonis, (2008), arXiv:0808.1220 [hep-ph].
 - [2] W. Roberts and M. Pervin, *Int. J. Mod. Phys.*, **A23**, 2817 (2008), arXiv:arXiv:0711.2492 [nucl-th].
 - [3] D. Ebert, R. Faustov, and V. Galkin, *Phys. Lett.*, **B659**, 612 (2008), arXiv:arXiv:0705.2957 [hep-ph].
 - [4] D. Ebert, R. Faustov, and V. Galkin, *Phys. Rev.*, **D72**, 034026 (2005), arXiv:hep-ph/0504112 [hep-ph].
 - [5] J.-R. Zhang and M.-Q. Huang, *Phys. Rev.*, **D78**, 094015 (2008), arXiv:0811.3266 [hep-ph].
 - [6] N. Mathur, R. Lewis, and R. Woloshyn, *Phys. Rev.*, **D66**, 014502 (2002), arXiv:hep-ph/0203253 [hep-ph].
 - [7] M. A. Ivanov, J. Korner, V. E. Lyubovitskij, and A. Rusetsky, *Phys. Lett.*, **B442**, 435 (1998), arXiv:hep-ph/9807519 [hep-ph].
 - [8] M. A. Ivanov, J. Korner, V. E. Lyubovitskij, and A. Rusetsky, *Phys. Rev.*, **D60**, 094002 (1999), arXiv:hep-ph/9904421 [hep-ph].
 - [9] S. Tawfiq, P. J. O'Donnell, and J. Korner, *Phys. Rev.*, **D58**, 054010 (1998), arXiv:hep-ph/9803246 [hep-ph].
 - [10] M.-Q. Huang, Y.-B. Dai, and C.-S. Huang, *Phys. Rev.*, **D52**, 3986 (1995).
 - [11] D. Pirjol and T.-M. Yan, *Phys. Rev.*, **D56**, 5483 (1997), arXiv:hep-ph/9701291 [hep-ph].
 - [12] J. L. Rosner, *Phys. Rev.*, **D52**, 6461 (1995), arXiv:hep-ph/9508252 [hep-ph].
 - [13] C. Amsler *et al.* (Particle Data Group), *Phys. Lett.*, **B667**, 1 (2008).
 - [14] M. Artuso *et al.* (CLEO Collaboration), *Phys. Rev.*, **D65**, 071101 (2002), arXiv:hep-ex/0110071 [hep-ex].
 - [15] J. Link *et al.* (FOCUS Collaboration), *Phys. Lett.*, **B525**, 205 (2002), arXiv:hep-ex/0111027 [hep-ex].
 - [16] G. Brandenburg *et al.* (CLEO Collaboration), *Phys. Rev. Lett.*, **78**, 2304 (1997).
 - [17] S. Athar *et al.* (CLEO Collaboration), *Phys. Rev.*, **D71**, 051101 (2005), arXiv:hep-ex/0410088 [hep-ex].
 - [18] H. Albrecht *et al.* (ARGUS Collaboration), *Phys. Lett.*, **B402**, 207 (1997).
 - [19] P. Frabetti *et al.* (E687 Collaboration), *Phys. Lett.*, **B365**, 461 (1996).
 - [20] K. Edwards *et al.* (CLEO Collaboration), *Phys. Rev. Lett.*, **74**, 3331 (1995).
 - [21] A. E. Blechman, A. F. Falk, D. Pirjol, and J. M. Yelton, *Phys. Rev.*, **D67**, 074033 (2003), arXiv:hep-ph/0302040 [hep-ph].
 - [22] The use of a specific particle state implies the use of the charge-conjugate state as well.
 - [23] D. E. Acosta *et al.* (CDF Collaboration), *Phys. Rev.*, **D71**, 032001 (2005), arXiv:hep-ex/0412071 [hep-ex].
 - [24] C. S. Hill (On behalf of the CDF Collaboration), *Nucl. Instrum. Meth.*, **A530**, 1 (2004).
 - [25] A. A. Affolder *et al.* (CDF Collaboration), *Nucl. Instrum. Meth.*, **A526**, 249 (2004).
 - [26] D. Acosta *et al.* (CDF-II), *Nucl. Instrum. Meth.*, **A518**, 605 (2004).
 - [27] E. J. Thomson, C. Ciobanu, J. Chung, J. Gerstenslager, J. Hoftiezer, *et al.*, *IEEE Trans. Nucl. Sci.*, **49**, 1063 (2002).
 - [28] D. Lange, *Nucl. Instrum. Meth.*, **A462**, 152 (2001).
 - [29] M. Feindt, (2004), arXiv:physics/0402093.
 - [30] M. Feindt and U. Kerzel, *Nucl. Instrum. Meth.*, **A559**, 190 (2006).
 - [31] M. Pivk and F. R. Le Diberder, *Nucl. Instrum. Meth.*, **A555**, 356 (2005), arXiv:physics/0402083.
 - [32] M. Pivk, (2006), arXiv:physics/0602023.
 - [33] E. Follana, C. Davies, G. Lepage, and J. Shigemitsu (HPQCD Collaboration, UKQCD Collaboration), *Phys. Rev. Lett.*, **100**, 062002 (2008), arXiv:arXiv:0706.1726 [hep-lat].
 - [34] T. Aaltonen *et al.* (CDF Collaboration), *Phys. Rev. Lett.*, **103**, 152001 (2009), arXiv:arXiv:0906.5218 [hep-ex].
 - [35] A. Abulencia *et al.* (CDF Collaboration), *Phys. Rev.*, **D73**, 051104 (2006), arXiv:hep-ex/0512069 [hep-ex].
 - [36] D. Aston *et al.*, *Nucl. Phys.*, **B296**, 493 (1988).
 - [37] S. Godfrey and N. Isgur, *Phys. Rev.*, **D32**, 189 (1985).